Electrodeposited Cobalt–Copper mixed oxides for supercapacitor electrodes and investigation of the Co/Cu ratio on the electrochemical performance

E. Noormohammadi[1,2] · S. Sanjabi[1] · F. Soavi[2] · F. Poli[2]

Abstract

In this study, different Cobalt–Copper mixed oxides compositions for supercapacitor electrodes have been prepared, by means of electrodeposition and thermal annealing. The chemical–physical and electrochemical characterization of electrodes, as well as the effect of different Co/Cu in the ratios on the crystal lattice, electrode morphologies, and electrochemical performance of the electrodes, were investigated using X-ray diffraction (XRD), scanning electron microscopic (SEM) and cyclic voltammetry (CV), electrochemical impedance spectroscopy (EIS), and galvanostatic charge/discharge (GCD) tests. The results indicated that the electrode prepared from 0.06 M $CoSO_4 \cdot 7H_2O + 0.04$ M $CuSO_4 \cdot 5H_2O$ solution (CC4) had a better electrochemical performance. The initial capacity of the CC4 electrode was 28.3 mAh/g at a scan rate of 5 mV/s with a coulombic efficiency of 94%. CC4 electrode featured capacity retention of 79.2% at a constant current density of 1 A/g after 5000 cycles.

Keywords Supercapacitor electrode · Cobalt–Copper mixed oxides · Electrodeposition · Electrochemical performance · Co/Cu ratio

Introduction

Supercapacitors are designed to meet the need for high power in a short time. In supercapacitors, the electrochemical energy is stored in the electrical field at the interface between the electrode and the electrolyte [1–5]. The key component of the supercapacitor electrode is its electrode material because all storage mechanisms depend on its type, structure, morphology, and amount in the electrode [6]. Electrical double-layer capacitors (EDLCs), pseudocapacitors (PCs), and battery-like supercapacitors are three types of supercapacitors, which are classified according to the charge-storage mechanism of the electrode material [6–8]. Transition metal oxides (TMOs) and their spinel structure as an electrode material to fabricate pseudocapacitors (PCs) and battery-like supercapacitors have attracted widespread research interest [9–11]. Transition metal oxides participate in energy storage through faradaic redox reactions, and their ability to perform these reactions is promoted by reducing their density and exposing a high surface of these materials to electrolytes [12]. Metal oxide spinel structures have attracted a lot of attention as a supercapacitor electrode material compared to single-component metal oxides due to their large ion diffusion pathways and the high surface of electrolyte exposure [13–18]. Along with research on other metal oxides, it has been widely demonstrated that cobalt spinels, especially copper–cobalt spinel ($CuCo_2O_4$), can be used as a suitable electrode material to improve the electrochemical performance of supercapacitors [19–21]. $CuCo_2O_4$ is a promising material for use in supercapacitors because this structure enables to exchange of a high number of electrons per mole of oxides as well as higher conductivity than that of copper oxide and cobalt oxide [22]. In this structure, copper compounds show high conductivity and cobalt compounds enhance energy storage capacity. Among the various methods deployed for spinel synthesis [23–30], electrochemical deposition is
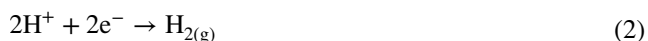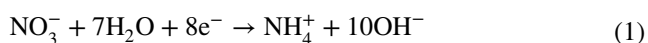
✉ S. Sanjabi
  Sanjabi@modares.ac.ir

1 Nanomaterials Group, Department of Materials Engineering, Tarbiat Modares University, Tehran 14115-143, Iran

2 Department of Chemistry ''Giacomo Ciamician'', University of Bologna, 40126 Bologna, Italy

considered a fast and direct preparation of the supercapacitor electrode method. Electrochemical deposition methods have been widely used due to easy composition control and high deposition rate as well as low cost compared to other multistep routs [30–32]. The formation and percentage of spinel phase in the coating structure depend on the synthesis method and the ratio of cobalt and copper elements during deposition. Despite many efforts have been devoted to the synthesis and use of $CuCo_2O_4$ spinel nanostructures for supercapacitor electrode materials, a clear identification of the best ratio of cobalt and copper that brings about the better spinel structure is still missing.

In this study, for the first time, we investigate the effect of different ratios of cobalt and copper on the electrochemical performance of $CuCo_2O_4$ electrodes for hybrid supercapacitors. We electrodeposited different compositions of Cobalt–Copper hydroxides on Ni foam (NF). The electrochemical deposition was carried out in a solution containing different rations of cobalt (II) and copper (II) sulfates in nitric acid. The reaction mechanism for the formation of Co–Cu hydroxide films is described by Eqs. (1)–(3) [32]:

$$NO_3^- + 7H_2O + 8e^- \rightarrow NH_4^+ + 10OH^- \tag{1}$$

$$2H^+ + 2e^- \rightarrow H_{2(g)} \tag{2}$$

$$xCu^{2+} + yCo^{2+} + 2(x+y)OH^- \rightarrow Cu_xCo_y(OH)_{2(x+y)} \tag{3}$$

$CuCo_2O_4$ was obtained by thermal annealing of electrodeposited Cobalt–Copper hydroxide films on NF as described by Eq. (4):

$$Cu_xCo_{2x}(OH)_{6x} + 1/2xO_2 \rightarrow xCuCo_2O_4 + 3H_2O \tag{4}$$
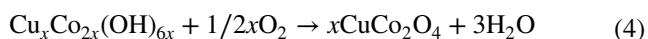
XRD and SEM analysis were used to investigate the phase structure and the surface morphology of electrodeposited electrodes, respectively. Cyclic voltammetry (CV), galvanostatic charge/discharge (GCD), cyclic stability test, and electrochemical impedance spectroscopy (EIS) were conducted to characterize the electrochemical performance of all prepared electrodes.

Materials and experimental methods

Materials

Cobalt (II) sulfate heptahydrate ($CoSO_4 \cdot 7H_2O$) and copper (II) sulfate pentahydrate ($CuSO_4 \cdot 5H_2O$), and Nitric acid ($\geq 65\%$) were purchased from Sigma-Aldrich. Nickel foam was provided by Goodfellow.

Preparation of cobalt oxide (CoO), copper oxide (CuO), and Cobalt–Copper mixed oxides coatings (CC)

Electrodeposition of Cobalt–Copper mixed oxides coating (CC; Table 1) was carried out from electrolyte solutions prepared from analytical grade chemicals (Sigma-Aldrich) and distilled water. Cobalt-containing coatings were obtained from aqueous solutions containing variable concentrations of $CoSO_4 \cdot 7H_2O$ and $CuSO_4 \cdot 5H_2O$ (Table 1). Pure cobalt oxide coating (CoO) was deposited from a 0.1 M $CoSO_4 \cdot 7H_2O$ aqueous solution. In order to adjust the pH to 1.4, HNO_3 was added to all solutions. Before electrodeposition, the Ni foam substrates measuring 0.25×0.25 cm^2 were cleaned with ethanol in an ultrasonic bath and dried in the atmosphere. The electrochemical process was performed in three-electrode cell consisting of a Pt mesh as a counter electrode, a Ni foam (NF) working electrode, and a Ti grid as a quasi-reference electrode. Under galvanostatic conditions with a current density of 1 A cm^{-2} for 45 s, the electrodeposition was run at room temperature. The average deposited mass of the oxide electrodeposited on Ni foam substrates was measured using Mettler Toledo balance and was 0.8 ± 0.1 mg. After drying, thermal annealing of the as-obtained samples was performed at 400 °C for 2 h under an unprotected atmosphere.

Material characterization

The phase structure of the electrodeposited coatings was investigated using high-resolution X-ray diffraction (XRD; PANalytical X'Pert PRO powder diffractometer equipped with an X'Celerator detector CuKα radiation, $\lambda = 1.5406$ Å, 40 mA, 40 kV). Morphological features and chemical composition of the samples were studied

Table 1 Sample identification and chemical composition

Sample ID	Targeted chemical composition/at %		Precursor concentration
	Cu	Co	
CoO	0	100	0.1 M $CoSO_4 \cdot 7H_2O$
CC2	20	80	0.08 M $CoSO_4 \cdot 7H_2O$ + 0.02 M $CuSO_4 \cdot 5H_2O$
CC4	40	60	0.06 M $CoSO_4 \cdot 7H_2O$ + 0.04 M $CuSO_4 \cdot 5H_2O$
CC6	60	40	0.04 M $CoSO_4 \cdot 7H_2O$ + 0.06 M $CuSO_4 \cdot 5H_2O$
CC8	80	20	0.02 M $CoSO_4 \cdot 7H_2O$ + 0.08 M $CuSO_4 \cdot 5H_2O$
CuO	100	0	0.1 M $CuSO_4 \cdot 5H_2O$

using scanning electron microscopy (SEM; Zeiss EVO 50 electron scanning microscope (SEM) equipped with an energy-dispersive X-ray analyzer (EDS) from Oxford INCA Energy 350 system.).

Electrochemical characterization

The electrochemical performances of all samples have been characterized in a three-electrode cell by cyclic voltammetry (CV) at different scan rates ranging from 5 to 200 mV s^{-1} at a potential window of -0.1 and 0.45 V (*vs.* Ag/AgCl), and GCD tests were performed in a 3 M KOH electrolyte between -0.1 and 0.45 V at a current density of 1 A g^{-1} to evaluate cycling stability. The electrochemical impedance spectroscopy (EIS) was measured in a 3 M KOH electrolyte over the frequency range 0.01–100 kHz, with 5 mV AC. All electrochemical measurements have been run with a (VSP multichannel potentiostat/galvanostat/FRA (Bio-Logic, Seyssinet-Pariset, France)) in a three-electrode cell configuration in which, the electrodeposited electrode was the working electrode, a Pt spring the counter, and Ag/AgCl the reference one.

Results and discussion

Structural and morphological analyses

XRD analysis was administrated on the coatings to see the crystalline phases present in each of them and therefore the results are depicted in Fig. 1. In Fig. 1, the peaks associated with the Ni foam substrate are indicated by "NF". Regarding the CoO sample (Fig. 1a), diffraction peaks can be observed at 31.2°, 36.8°, 44.8°, 59.3°, and 65.2° indexed to the (220), (311), (400), (511), and (440) planes of the cubic phase of Co$_3$O$_4$ which is in agreement with standard JCPDS data [31, 32]. CuO sample shows well-defined peaks at different angles which are marked with a black symbol in Fig. 1a. consistent with the XRD pattern of CuO, there are two sharper diffraction peaks located at 35.5° and 38.6° corresponding to the (002) and (111) planes of monoclinic CuO structure. Figure 1b presents the patterns of the Cobalt–Copper mixed oxides (CC) coatings, which are drawn in several colors and from CC8 to CC2, respectively. As shown within the Fig. 1b, peaks associated with copper oxide appeared more sharply in samples obtained from Cu-rich solutions (CC8 and CC6), whereas with the rise of cobalt in solution (CC4 and CC2), the intensity of those peaks gradually decreases, and peaks associated with cobalt oxide and Cobalt–Copper spinel structure appear. The peaks indicated with a black symbol are indexed to the (111), (220), (311), (400), (511), and (440) planes of the spinel cubic CuCo$_2$O$_4$ phase, respectively (JCPDS card no. 01–1155). Additionally, the main
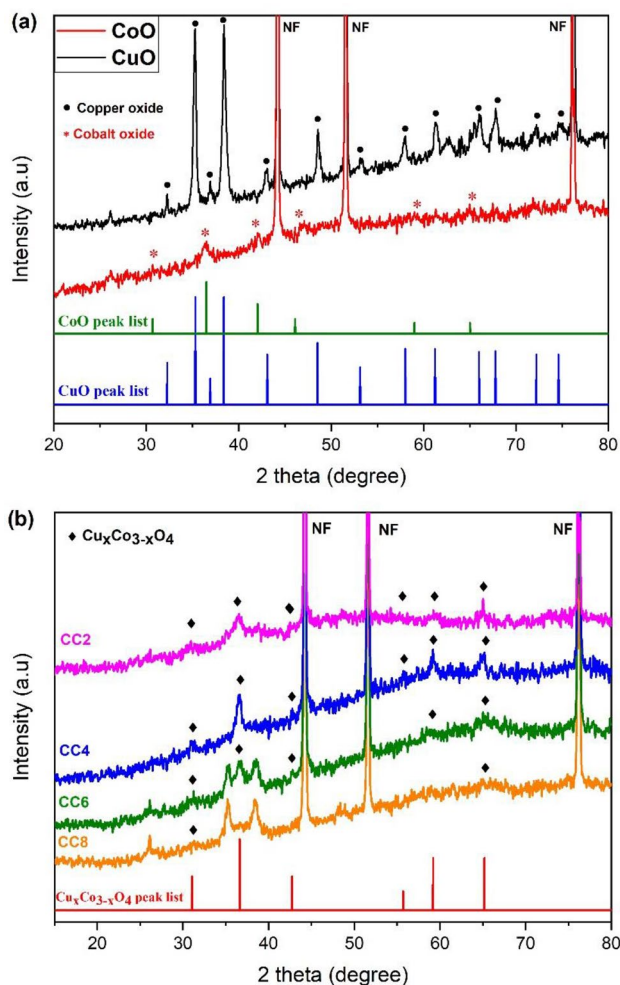

Fig. 1 X-ray diffraction patterns of **a** cobalt oxide (CoO) and copper oxide (CuO) and **b** Cobalt–Copper mixed oxides (CC2, CC4, CC6 and CC8) deposited on NF, compared with the reference XRD pattern of the spinel Cu$_x$Co$_{3-x}$O$_4$ (in red)

peaks of the Cu$_x$Co$_{3-x}$O$_4$ spinel structure appeared within the diffraction pattern of all mixed oxides samples. Table 2 shows the intensity, location and corresponding plane of the three main peaks of Cu$_x$Co$_{3-x}$O$_4$ spinel structure for each sample. According to the table and comparison of intensity values, it is well understood that the spinel phase peaks are more evident within the CC4 sample, indicating that more spinel phase has been formed in this coating. These results are consistent with previous reports [32–34].

Figure 2 shows low and high magnification SEM images of all electrodeposited coatings, which are arranged from the CoO electrode to the CuO electrode, respectively, based on the increase in the amount of copper in the coating. Morphological features such as particle size, growth process, structure, and pores created are different depending on the composition of cobalt and copper. Figure 2b reveals that in the CoO layer, particles are placed
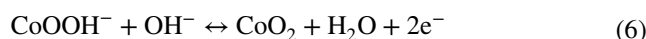
Table 2 The intensity, location and corresponding plane of the three main peaks of $Cu_xCo_{3-x}O_4$ spinel structure for all samples

Peak position (°2theta)	CC2		CC4		CC6		CC8	
	Intensity (cts)	Plane	Intensity (cts)	Plane	Intensity (cts)	Plane	Intensity (cts)	Plane
36.61	368.21	{220}	526.30	{220}	240.22	{220}	286.93	{220}
59.174	328.34	{511}	486.76	{511}	308.11	{511}	230.65	{511}
65.192	357.52	{440}	479.16	{440}	337.5	{440}	253.19	{440}

alongside one another to create interconnected fractal structures with a length of 100 μm and grow into cauliflower form. As shown in Fig. 2a, b, and c, samples with higher cobalt content display cauliflower-like structures with sharp surfaces and smaller pores, while samples with more copper content show larger pores with open dendritic walls. (Fig. 2d, e, and f). Dendrites do not present any preferential growth (in relevancy the substrate); they are randomly oriented. In addition, the porous structure created within the coatings is due to hydrogen bubbles on the surface during electrodeposition. The constant evolution of H_2 bubbles during the deposition limits the free volume available for metal(s) growth, forcing it to occur around the evolving bubbles. The concentration of elements in all samples which is taken by EDS can be observed in Fig. 2g. Sample identification and average Co/Cu composition ratio of CC2 to CC8 electrodes as determined by EDS are presented in Table 3. The EDS results confirm the targeted compositions in cobalt and copper.

Electrochemical characterization

To evaluate the electrochemical performance of all samples, cyclic voltammetry (CV), galvanostatic charge/discharge (GCD), and electrochemical impedance spectroscopy (EIS) measurements were conducted in 3 M KOH aqueous solution employing a three-electrode system. CV experiments have been run to investigate both the occurrence of reversible faradaic reaction at the electrode and an acceptable potential range with high coulombic efficiency. Figure 3a shows CV curves of all electrodes at 5 mV/s at which redox peaks contributed from the faradaic reactions are observed. The non-rectangular behavior of all CV curves confirms that Faradaic reactions occur at the surface of the electrodes and also the charge-storage mechanism is principally because of these reactions. Within the cathodic scan, redox peaks are clearly observed in copper–cobalt mixed oxide (CC) and CoO electrodes at the potentials of approximately 0.36 and 0.28 V *vs.* Ag/AgCl which indicates the characteristic of a battery-like electrode for all of them. These redox peaks are attributed to the couples Co^{3+}/Co^{2+} and Cu^{2+}/Cu^+ reactions taking place in KOH electrolyte. [35]. The expected reaction equations are as follows (5)–(7) [32, 36]:

$$CuCo_2O_4 + H_2O + e^- \leftrightarrow 2CoOOH^- + Cu(OH)^+ \quad (5)$$

$$CoOOH^- + OH^- \leftrightarrow CoO_2 + H_2O + 2e^- \quad (6)$$

$$CuOH^+ + e^- \leftrightarrow Cu(OH) \quad (7)$$

The cyclic voltammogram curves (CV) for the CC4 electrode at different scan rates starting from 5 to 200 mV/s are shown in Fig. 3b. A slight shift of the anodic and cathodic peaks towards higher and lower potential is observed with increasing scan rate. This was due to the slow kinetics of electrolyte ion transport within the active layer at high scan rates [37]. In addition, as the scan rate is increased from 5 to 200 mV s^{-1}, the shapes of these CV curves do not show significant change implying the wonderful reversibility of the Faradaic redox reaction. The enclosed area of the CV curves is indicative of the electrode capacity, which is broadener for the CC4 electrode, confirming the maximum capacity provided by CC4 compared to other electrodes. Based on the integral of the CV cathodic current over time, the specific capacity of the electrodes was calculated, using Eq. (8) [32]:

$$Q_s = \frac{1}{(3.6\,m)} \int_{t_i}^{t_f} I\,dt \quad (8)$$

where m is the mass of the materials.

Since these electrodes exhibited redox peaks in the CV curve and the capacitance of the electrodes varies over the whole potential window, the interpretation of these electrodes must be different from that of pseudocapacitive, and the term of specific capacity Qs (mAh/g) must be used to evaluate their electrochemical performance [38]. The calculated specific capacity of the electrodes as a function of scan rate has been shown in Fig. 3c. The specific capacity decreases with increasing scan rate due to the redox reaction on the electrode surface [39]. According to Fig. 3c, the electrodes containing more copper than cobalt showed less capacity, and the capacity of the CC4 electrode had the highest value at each scan rate. The maximum specific capacity of the CC4 electrode is 28.3 mAh/g at 5 mV s^{-1}. The calculated specific capacity values for CuO, CoO,

Fig. 2 SEM images for **a** CoO,
b CC2, **c** CC4, **d** CC6, **e** CC8, **f**
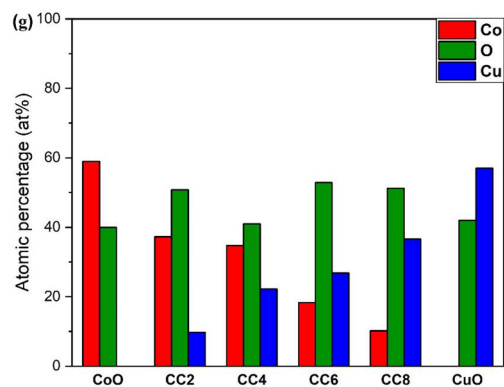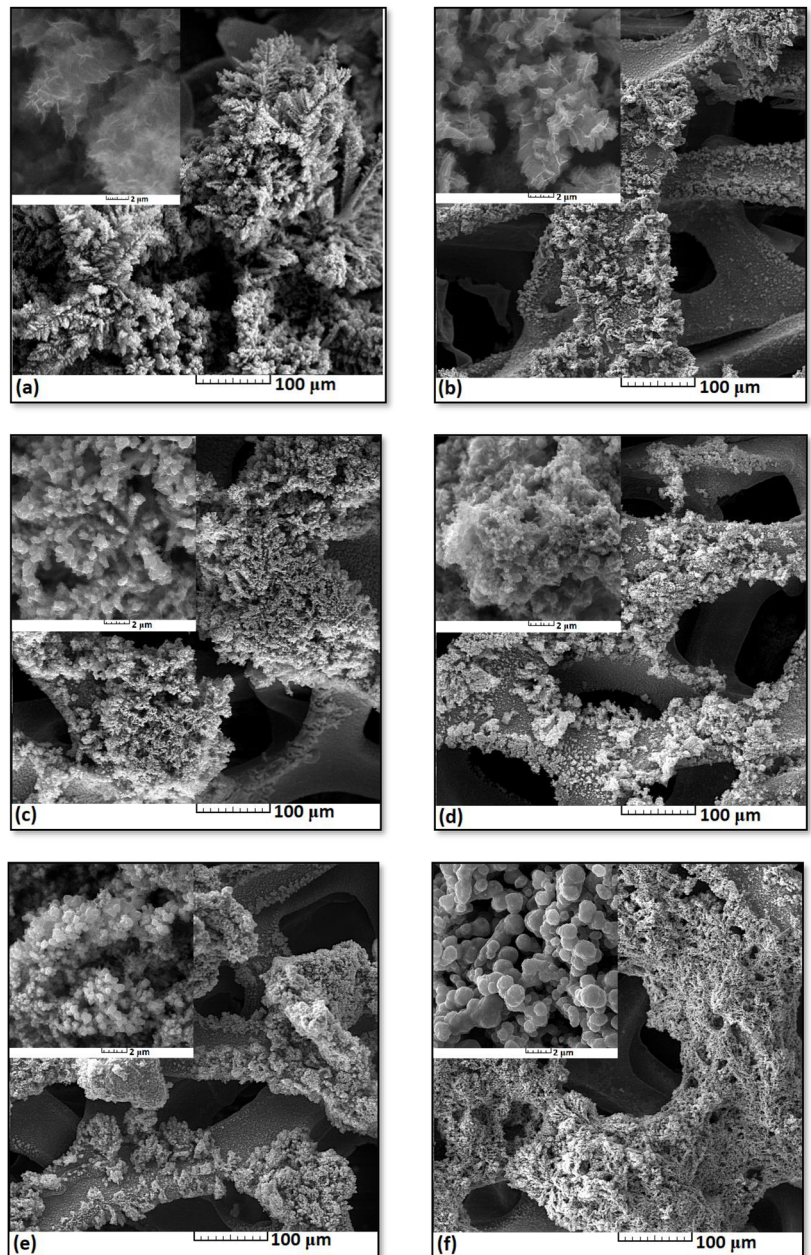CuO, and **g** elements composition in all samples using EDS

Table 3 Targeted and determined Co/Cu composition ratio of CC2 to CC8 electrodes

Sample ID	Targeted Co/Cu composition ratio	Co/Cu composition ratio as determined by EDS
CC2	4	3.82
CC4	1.5	1.56
CC6	0.66	0.69
CC8	0.25	0.27

CC8, CC6, and CC2 were found to be 8.3, 12.7. 15.4, 23.3, and 18.7 mAh/g, respectively at 5 mV/s.

Figure 3d reports the values of coulombic efficiency of the electrodes at different scan rates. The highest coulombic efficiencies, of 96%, for CC4, were achieved in the potential range of − 0.1 to 0.45 V vs Ag/AgCl. By increasing the scan rate, the coulombic efficiency of all electrodes increases, but the CC4 electrode features higher efficiency at all scan rates and underwent a uniform trend at higher scan rates.

The change in anodic and cathodic peak currents with respect to square roots of scan rates of the CC4 electrode are plotted and shown in Fig. 3e and it showed linear in nature which is expounded to the mass diffusion control process [40, 41].

This conclusion is further confirmed by the subsequent galvanostatic charge–discharge tests. Figure 4a reports the galvanostatic charge/discharge curves of all electrodes at a density of 1 A/g with a potential range of − 0.1 to 0.45 V. GCD is a reliable method for evaluating the electrochemical capacity of materials under controlled conditions. Nonlinear discharge curves of the electrode potential profile confirmed the Faradaic behavior of the battery-like electrode. In order to calculate the specific capacity of the electrodes from the galvanostatic discharge curves, Eq. (9) was used [32]:

$$Q_s = \frac{I \times \Delta t}{m} \tag{9}$$

where I is the current (A), m is the mass loading of the oxide materials on the electrode (g) and Δt is the discharge time (s).

According to the GCD curves, there is a linear change of potential with the charge in the potential range of 0.4–0.2 V vs Ag/AgCl. Therefore, only within this range the electrodes can be interpreted as a pseudocapacitor. Using the slope of the discharge curve, the specific capacitance of all electrodes is estimated to be 315, 219, 170, 157, 113, and 56 F/g for CC4, CC2, CoO, CC6, CC8, and CuO, respectively. These results are fairly consistent with the results observed in the CV curves.

Since these results clearly indicated that the electrochemical performance of the CC4 electrode was much better than other electrodes, the performance of the long-term cycling stability and ion transport properties of the CC4 electrode was evaluated and is shown in Fig. 4b, c. The cycling measurements were carried out at a current density of 1 A g^{-1} for 5000 cycles in 3 M KOH, at which the CC4 electrode shows good cycling stability with a capacity retention of ~79.2% in 3 M KOH.

The electronic and ionic conductivities and diffusive behavior of the electrodes were investigated using EIS analysis. Figure 4c compares the Nyquist plots of the CC4 and CC2 electrodes. A semicircle in the high-frequency region and a straight line in the low-frequency region show that the Nyquist plots of these electrodes are closer to an ideal supercapacitor. The figure inset is the magnification of the plots at the highest frequencies. The high-frequency intercept of the semicircle on the real axis indicates the uncompensated resistance including the electrode electronic resistance and the electrolyte ionic resistance, and that depends on the electrochemical cell geometry. The straight line in the low-frequency region is related to the Warburg impedance (ZW) and the semicircle is associated with the diffusion of ions into the electrode and the charge transfer resistance (Rct), respectively [42]. The CC4 electrode has lower high-frequency resistance (1.1 ohms) than the CC2 electrode (1.4 ohms). According to these data and considering that these two measurements were performed using the same electrolyte and cell configuration, it can be argued that the lower resistance of CC4 is related to its better conductivity achieved by more spinel phase and the resulting defects in the coating structure. In addition, the slope of the Warburg line of the CC4 sample was slightly higher than that of the CC2, which can be attributed to the difference between the two samples in porosity, reactivity, and the number of defects due to the spinel phase, which decreased the resistance to electron/ion diffusion and increased the redox reactions at the electrode.

Conclusion

In summary, supercapacitor electrodes of the Cobalt–Copper mixed oxides (CC) with different ratios of Co/Cu were synthesized on nickel foam by electrochemical deposition. X-ray diffraction showed the presence of Cobalt–Copper oxide spinel structure and the electrode synthesized from 0.06 $CoSO_4 \cdot 7H_2O$ + 0.04 M $CuSO_4.5H_2O$ solution (CC4) featured a higher content of the spinel phase of $CuCo_2O_4$. SEM images of samples approved the simultaneous presence of Co and Cu and morphological and structural changes due to differences in the composition of cobalt and copper in the coatings. Electrochemical examinations indicated that the CC4 electrode had a higher specific capacity and better electrochemical performance compared to other electrodes. The initial capacity of the CC4 electrode was 28.3 mAh/g at
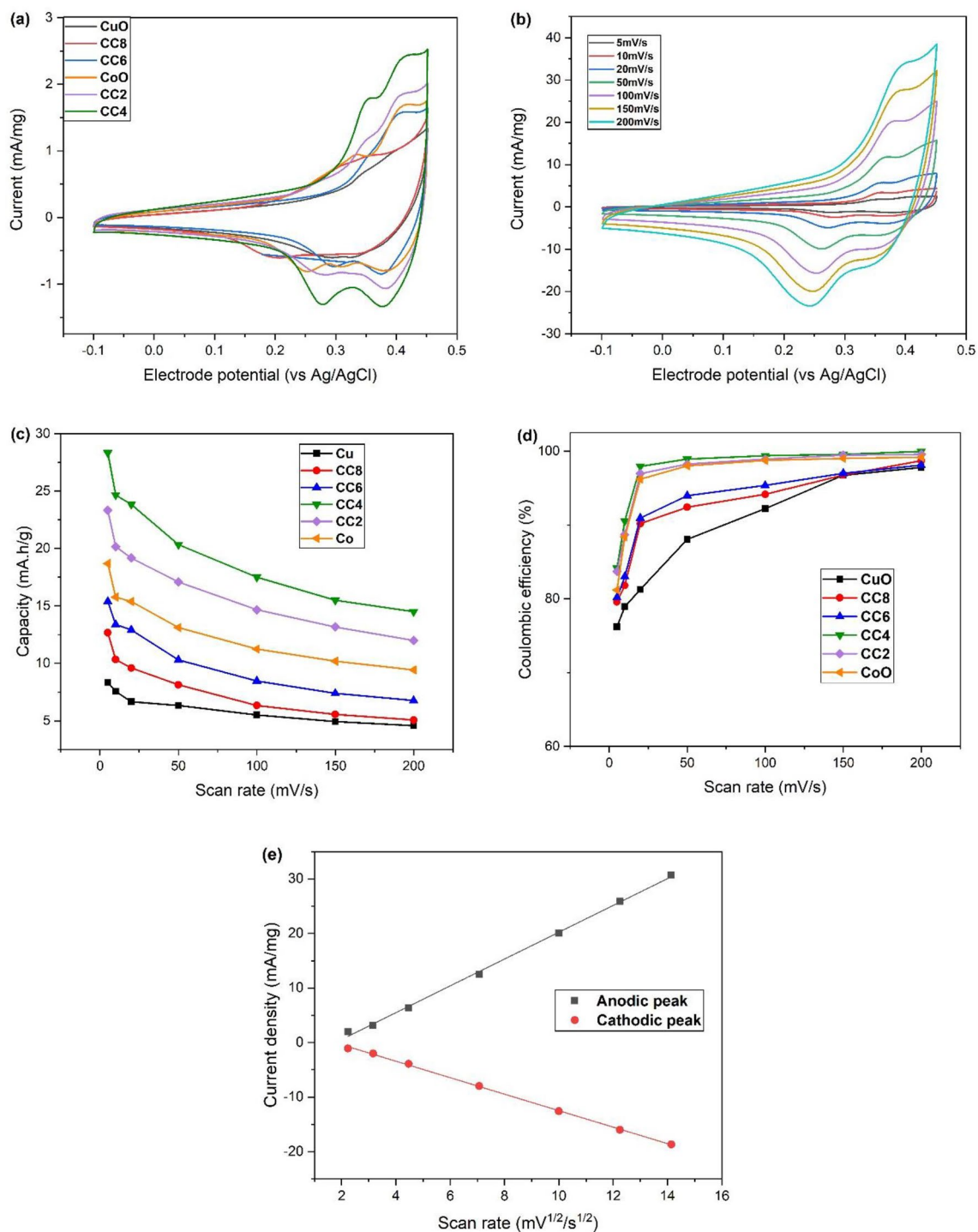
Fig. 3 **a** comparison of the CV of all electrodes at 5 mV/s, **b** CV of CC4 electrode at different scan rates, **c** CV capacity of electrodes at different scan rates, **d** coulombic efficiency of electrodes at different scan rates, and **e** plots of the cathodic and anodic peaks of current densities obtained from (**a**, **b**) versus (scan rate)$^{1/2}$
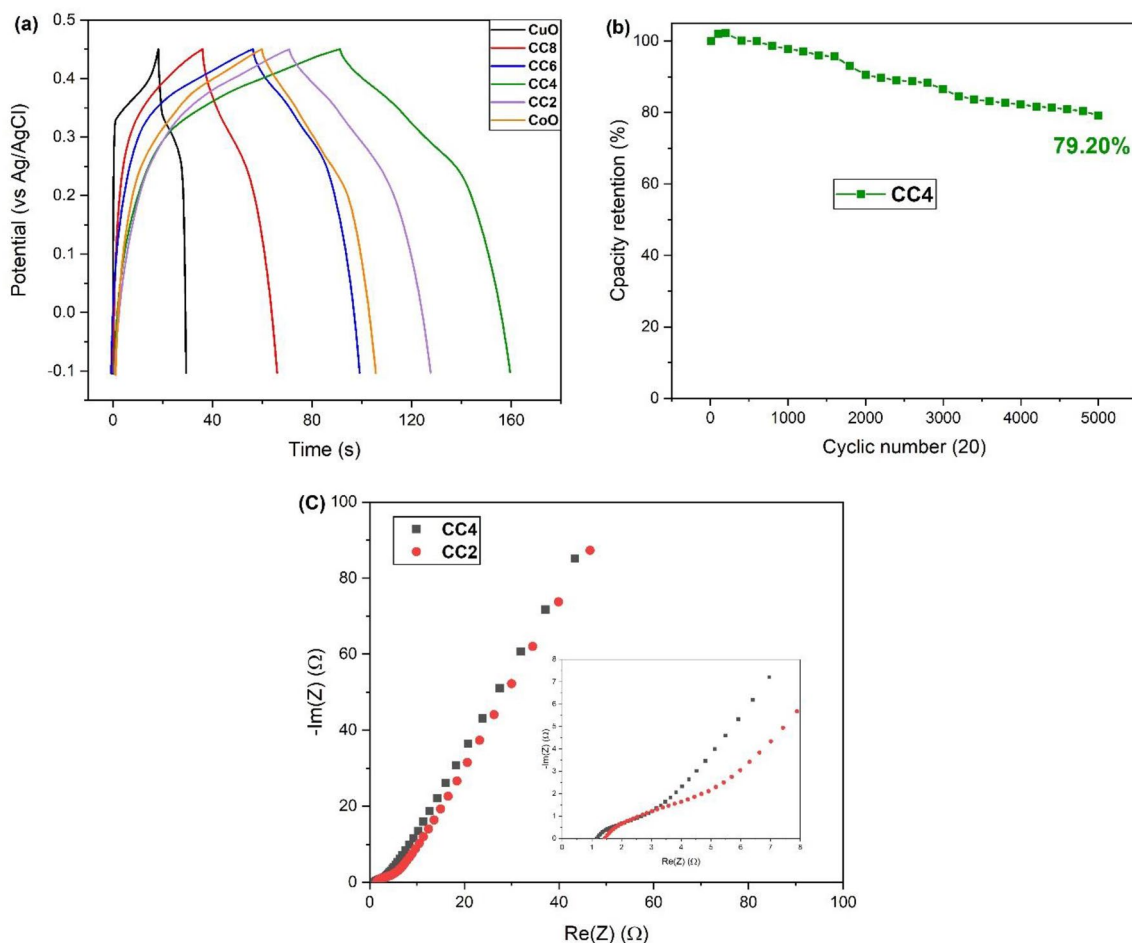
Fig. 4 **a** GCPL profiles of electrodes at 1 A/g, **b** capacity retention of CC4 electrode, and **c** Nyquist plot of the CC4 electrode

a scan rate of 5 mV/s with a coulombic efficiency of 94%. In addition, it showed capacity retention of 79.2% at a constant current density of 1 A/g after 5000 cycles.

Declarations

Conflict of interest The authors have no conflict of interest to declare.

References

1. Bavio, M.A., Acosta, G.G., Kessler, T.: Synthesis and characterization of polyaniline and polyaniline-carbon nanotubes nanostructures for electrochemical supercapacitors. J. Power Sources **245**, 475–481 (2014)
2. Jiang, Y., Chen, L., Zhang, H., Zhang, Q., Chen, W., Zhu, J., Song, D.: Two-dimensional Co_3O_4 thin sheets assembled by 3D interconnected nanoflake array framework structures with enhanced supercapacitor performance derived from coordination complexes. Chem. Eng. J. **292**, 1 (2016)
3. Whittingham, M.S., Zawodzinski, T.: Introduction: batteries and fuel cells. Chem. Rev. **104**, 4243–4244 (2004)
4. Kim, M., Kim, J.: Development of high power and energy density microsphere silicon carbide–MnO_2 nanoneedles and thermally oxidized activated carbon asymmetric electrochemical supercapacitors. Phys. Chem. Chem. Phys. **16**, 11323 (2014)
5. Zhai, Y., Dou, Y., Zhao, D., Fulvio, P.F., Mayes, R.T., Dai, S.: Carbon materials for chemical capacitive energy storage. Adv. Mater. **22**, 4828 (2011)
6. Simon, P., Gogotsi, Y.: Materials for electrochemical capacitors. Nature Mat **7**, 845–854 (2008)

☒ Springer

7. Dunn, B., Kamath, H.: Electrical energy storage for the grid: a battery of choices. J. M. Tarascon. Science. **334**, 928 (2011)

8. Wang, T., Chen, H., Yu, F., Zhao, X., Wang, H.: Boosting the cycling stability of transition metal compounds-based supercapacitors. Energy Stor. Mater. **16**, 545–573 (2019)

9. Xia, X.-H., Tu, J.-P., Zhang, Y.-Q., Mai, Y.-J., Wang, X.-L., Gu, C.-D., Zhao, X.-B.: Freestanding Co_3O_4 nanowire array for high performance supercapacitors. RSC Adv. **2**, 1835–1841 (2012)

10. Wang, Q., Yan, J., Fan, Z.: Carbon materials for high volumetric performance supercapacitors: design, progress, challenges and opportunities. Energy Environ Sci. **9**, 729–762 (2016)

11. Zhang, K., Zeng, W., Zhang, G., Hou, S., Wang, F., Wang, T., Duan, H.: Hierarchical $CuCo_2O_4$ nanowire@$NiCo2O4$ nanosheet core/shell arrays for high-performance supercapacitors. RSC Adv. **5**, 69636–69641 (2015)

12. Pell, W., Conway, B.: Peculiarities and requirements of asymmetric capacitor devices based on combination of capacitor and battery-type electrodes. J. Power Sources **136**, 334–345 (2004)

13. Chen, D., Wang, Q., Wang, R., Shen, G.: Ternary oxide nanostructured materials for supercapacitors: a review. J. Mater. Chem. **3**, 10158–10173 (2015)

14. Lukatskaya, M.R., Kota, S., Lin, Z., Zhao, M.Q., Shpigel, N., Levi, M.D., Halim, J., Taberna, P.L., Barsoum, M.W., Simon, P.: Ultra-high-rate pseudocapacitive energy storage in two-dimensional transition metal carbides. Nat. Energy **2**, 17105 (2017)

15. Chandra Sekhar, S., Nagaraju, G., Yu, J.S.: High-performance pouch-type hybrid supercapacitor based on hierarchical NiO–Co_3O_4–NiO composite nanoarchitectures as an advanced electrode material. Nano Energy **48**, 81–92 (2018)

16. Xu, Y., Liu, Z., Chen, D., Song, Y., Wang, R.: Synthesis and electrochemical properties of porous α-$Co(OH)_2$ and Co_3O_4 microspheres. Prog. Nat. Sci. **27**, 197–202 (2017)

17. Pendashteh, A., Moosavifard, S.E., Rahmanifar, M.S., Wang, Y., Elkady, M.F., Kaner, R.B., Mousavi, M.F.: Highly ordered mesoporous $CuCo_2O_4$ nanowires, a promising solution for high-performance supercapacitors. Chem. Mater. **39**, 3919–3926 (2015)

18. Nithya, V.D., Arul, N.S.: Review on a-Fe_2O_3 based negative electrode for high performance supercapacitors. J. Power Sources **327**, 297–318 (2016)

19. Vijayakumar, S., Lee, S.H., Ryu, K.S.: Hierarchical $CuCo_2O_4$ nanobelts as a supercapacitor electrode with high areal and specific capacitance. Electrochim Acta **182**, 979–986 (2015)

20. Kaverlavani, S.K., Moosavifard, S.E., Bakouei, A.: Designing graphene-wrapped nanoporous $CuCo_2O_4$ hollow spheres electrodes for high-performance asymmetric supercapacitors. J. Mater. Chem. A **5**, 14301–14309 (2017)

21. Sun, J., Chunju, Xu., Chen, H.: A review on the synthesis of $CuCo_2O_4$-based electrode materials and their applications in supercapacitors. J. Materiomics **7**, 98–126 (2021)

22. Ge, H., Wang, C., Yin, L.: Hierarchical $Cu_{0.27}Co_{2.73}O_4$/MnO_2 nanorod arrays grown on 3D nickel foam as promising electrode materials for electrochemical capacitors. J. Mater. Chem. A **3**, 17359–17368 (2015)

23. Wang, Q., Xu, J., Wang, X., Liu, B., Hou, X., Yu, G., Wang, P., Chen, D., Shen, G.: CoreShell $CuCo_2O_4$@MnO_2 nanowires on carbon fabrics as high-performance materials for flexible, all solid-state, electrochemical capacitors. Chem. Electro. Chem. **1**, 559–564 (2014)

24. Kuang, M., Liu, X.Y., Dong, F., Zhang, Y.X.: Tunable design of layered $CuCo_2O_4$ nanosheets@$MnO2$ nanoflakes core-shell arrays on Ni foam for high performance supercapacitors. J. Mater. Chem. A. **3**, 21528–21536 (2015)

25. Naik, K.K., Sahoo, S., Rout, C.S.: Facile electrochemical growth of spinel copper cobaltite nanosheets for non-enzymatic glucose sensing and supercapacitor applications. Microporous Mesoporous Mater. **244**, 226–234 (2017)

26. Reddy, M., Yu, C., Jiahuan, F., Loh, K.P., Chowdari, B.: Molten salt synthesis and energy storage studies on $CuCo_2O_4$ and $CuOCo_3O_4$. RSC Adv. **2**, 9619–9625 (2012)

27. Alizadeh-Gheshlaghi, E., Shaabani, B., Khodayari, A., Azizian-Kalandaragh, Y., Rahimi, R.: Investigation of the catalytic activity of nano-sized CuO, Co_3O_4 and $CuCo_2O_4$ powders on thermal decomposition of ammonium perchlorate. Powder Technol. **217**, 330–339 (2012)

28. Liu, Y., Cao, L.J., Cao, C.W., Wang, M., Leung, K.L., Zeng, S.S., Hung, T., Chung, C., Lu, Z.G.: Facile synthesis of spinel $CuCo_2O_4$ nanocrystals as high-performance cathode catalysts for rechargeable Li–air batteries. Chem. Commun. **50**, 14635–14638 (2014)

29. Wang, Y., Shen, C., Niu, L., Li, R., Guo, H., Shi, Y., Li, C., Liu, X., Gong, Y.: Hydrothermal synthesis of $CuCo_2O_4$/CuO nanowire arrays and RGO/Fe_2O_3 composites for high-performance aqueous asymmetric supercapacitors. J. Mater. Chem. A. **4**, 9977–9985 (2016)

30. Gomez, E., Labarta, A., Llorente, A., Valles, E.: "Electrodeposited cobalt + copper thin films on ITO substrate. J. Electroanal. Chem. **517**, 63–68 (2001)

31. Gomez, E., Llorente, A., Alcobe, X., Valles, E.: Electrodeposition for obtaining homogeneous or heterogeneous Cobalt-Copper films. J. Solid State Eletro. Chem. **8**, 82–88 (2004)

32. Noormohammadi, E., Poli, F., Durante, C., Lunardon, M., Sanjabi, S., Soavi, F.: Electrodeposition of cobalt–copper oxides decorated with conductive polymer for supercapacitor electrodes with high stability. ChemElectroChem **9**, e202200102 (2022)

33. Sharma, Y., Sharma, N., Subba Rao, G.V., Chowdari, B.V.R.: Lithium recycling behaviour of nano-phase-$CuCo_2O_4$ as anode for lithium-ion batteries. J. Power Sources **173**, 495 (2007)

34. Pendashteh, A., Rahmanifar, M.S., Kaner, R.B., Mousavi, M.F.: Facile synthesis of nanostructured $CuCo_2O_4$ as a novel electrode material for high-rate supercapacitors. Chem. Commun. **50**, 1972 (2014)

35. Nath, N.C.D., Debnath, T., Eun-Kyung Kim, M.D., Shaikh, A.A., Lee, J.-J.: Nanostructured copper–cobalt based spinel for the electrocatalytic H_2O_2 reduction reaction. Electrochim. Acta **273**, 474–482 (2018)

36. Zhang, L., Li, R., Li, W., Li, R., Li, C., Zhou, Y.: $CuCo_2O_4$ nanoneedle array with high stability for high performance asymmetric supercapacitors. RSC Adv. **10**, 22775–22782 (2020)

37. Cai, D., Wang, D., Liu, B., Wang, L., Liu, Y., Li, H., Wang, Y., Li, Q., Wang, T.: Three-dimensional Co_3O_4@ $NiMoO_4$ core/shell nanowire arrays on ni foam for electrochemical energy storage. ACS Appl. Mater. Interfaces. **6**, 5050–5055 (2014)

38. Gogotsi, Y., Penner, R.M.: Energy storage in nanomaterials-capacitive, pseudocapacitive, or battery-like? ACS Nano **12**, 2081–2083 (2018)

39. Jadhav, H.S., Pawar, S.M., Jadhav, A.H., Thorat, G.M., Seo, J.G.: Hierarchical mesoporous 3D flower-like $CuCo_2O_4$/NF for high-performance electrochemical energy storage. Sci. Rep. **6**, 31120 (2016)

40. Srivastava, R.K., Srivastava, S., Narayanan, T.N., Mahlotra, B.D., Vajtai, R., Ajayan, P.M., Srivastava, A.: Functionalized multilayered graphene platform for urea sensor. ACS Nano **6**, 168 (2012)

41. Zou, Y., He, L., Dou, K., Wang, S., Ke, P., Wang, A.: Amperometric glucose sensor based on boron doped microcrystalline diamond film electrode with different boron doping levels. RSC Adv. **4**, 58349 (2014)

42. Inamdar, A.I., Kalubarme, R.S., Kim, J., Jo, Y., Woo, H., Cho, S., Pawar, S.M., Park, C.J., Lee, Y.W., Sohn, J.I., Cha, S., Kwak, J., Kim, H., Im, H.: Nickel titanate lithium-ion battery anodes with high reversible capacity and high-rate long-cycle life performance. J. Mater. Chem. A. **4**, 4691 (2016)